

# Fine structure of the 0.7 MeV resonance in the $^{230}\text{Th}$ neutron-induced cross section

## Short title: Fine structure in neutron-induced fission

M. MIREA<sup>1</sup>, L. TASSAN-GOT<sup>2</sup>, C. STEPHAN<sup>2</sup>, C.O. BACRI<sup>2</sup> and R.C. BOBULESCU<sup>3</sup>

<sup>1</sup> *Institute of Physics and Nuclear Engineering - P.O. Box MG-6, Bucharest, Romania*

<sup>2</sup> *Institut de Physique Nucléaire - 91406 Orsay-Cedex, France*

<sup>3</sup> *Faculty of Physics, P.O. Box MG-11, Bucharest, Romania*

PACS. 24.10.-i – Nuclear reaction models and methods.

PACS. 24.75.+i – General properties of fission.

PACS. 25.85.Ec – Neutron-induced fission.

**Abstract.** – The fine structure of the 0.7 MeV resonance in the  $^{230}\text{Th}$  neutron-induced cross section is investigated within the hybrid model. A very good agreement with experimental data is obtained. It is suggested that fine structure of the cross section quantify the changes of the intrinsic states of the nucleus during the disintegration process.

*Introduction.* – The neutron-induced cross sections of  $^{230,232}\text{Th}$  exhibit multiple fine structures [1, 2] superimposed on a gross structure of the threshold cross section. If the fine structure is interpreted as a series of rotational states constructed on a  $\beta$ -vibrational state produced in some well of the multidimensional barrier, it is straightforward to postulate the existence of a triple humped barrier. The spacing between the members of the band is so small that it is consistent only with a parent nucleus with prolate deformation that reaches the vicinity of the second barrier top. Therefore, a shallow minimum can be expected at this deformation to create a  $\beta$ -vibrational state. Up to now, the assumption of a triple humped barrier seems to be the best interpretation for the fine structure of intermediate cross section resonances [3]. The principal aim of the present work is to offer an alternative explanation of this phenomenon by taking into account dynamical single-particle effects.

Recently, a Hybrid Model (HM) [4] was developed in order to investigate the intermediate structure of the fission cross section. In the frame of the HM, the excited states during the deformation process of the parent nucleus and their realization probabilities must be obtained. The occupations of the excited states are determined theoretically by solving microscopic equations of motion. These excited states are added to a phenomenological double humped barrier and new barriers with different shapes are constructed. The energy width in the fission channel is proportional to the weighted summation of the penetrabilities of these barriers. The fine structure of the 0.7 MeV resonance of the  $^{230}\text{Th}$  neutron-induced cross section is studied within our model.

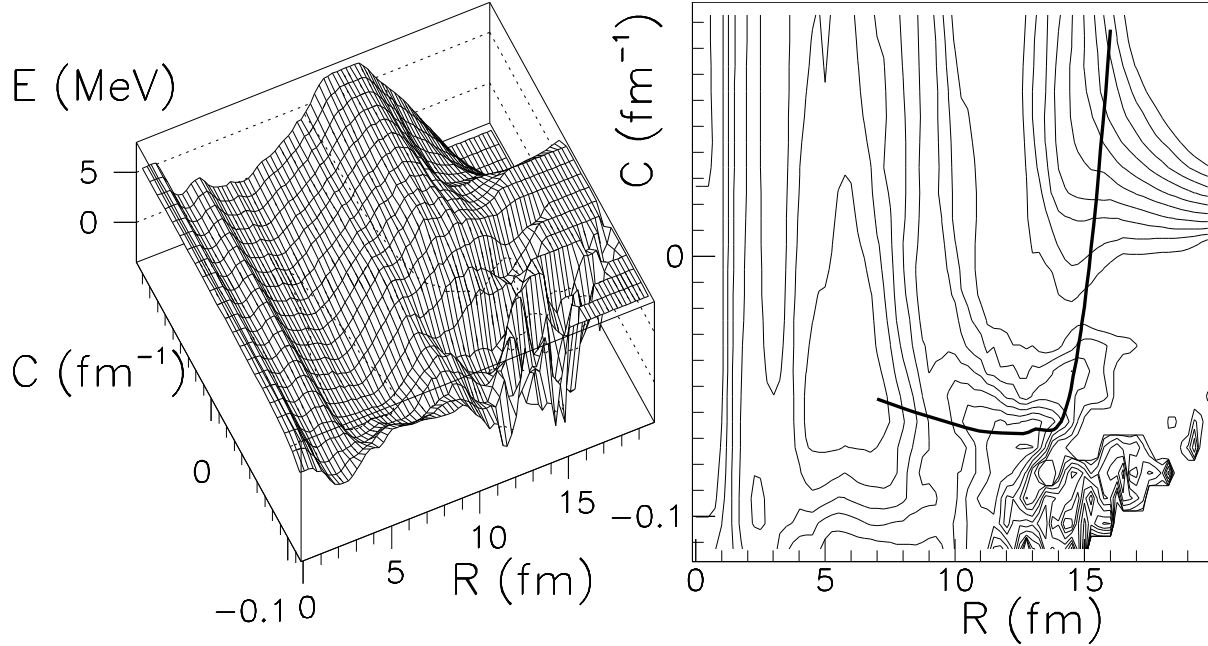


Fig. 1 – Deformation energy in MeV for the partition  $^{231}\text{Th} \rightarrow ^{100}\text{Zr} + ^{131}\text{Sn}$ .  $C$  represents the curvature of the neck and  $R$  is the distance between the centers of the fragments. The mass-asymmetry parameter is varied linearly with  $R$  from 0 (in the ground-state configuration) up to the final value (at the exit point of the barrier). In the right panel the step between two equipotential lines is 1 MeV. The best action trajectory is represented with a thick line that starts in the first well, penetrates the first barrier, attains the second well and tunnels the second barrier towards scission. Positive values of  $C$  characterize necked-in shapes while negative values correspond to neck-swollen shapes.

*Formalism.* – Details concerning the HM can be found in ref. [4] and only the main steps that focus strictly on the  $^{230}\text{Th}$  neutron-induced cross section will be underlined in the following.

In order to determine the intrinsic single-particle states and their associated occupation probabilities during the fission process it is necessary to perform a full calculation of the trajectory of the decaying system in the available configuration space. For this purpose, an axial-symmetric nuclear shape parametrization given by two spheres of different radii smoothly joined by a neck region is used. This nuclear shape parametrization depends on the most important macroscopic degrees of freedom encountered in fission, namely elongation, necking and mass-asymmetry. The deformation energy is obtained as a sum between the liquid drop energy and the shell effects. The fission trajectory can be obtained by minimizing the action integral in the tridimensional configuration space. In fig. 1, the deformation energy for the  $^{231}\text{Th}$  fission with heavy fragment  $^{131}\text{Sn}$  is displayed together with the best trajectory. In this work, the liquid drop energy is obtained in the frame of the Yukawa-plus-exponential model extended for binary systems with different charge densities [5]. The shell effects are determined using the Strutinsky prescriptions acting on level schemes constructed with the Superasymmetric Two-Centre Shell Model (STCSM) [6]. The STCSM supplies single-particle states by adding correction terms to a double oscillator eigenstates. In the STCSM, the most important terms to be diagonalized are: the mass-asymmetry one, the neck one, the spin-

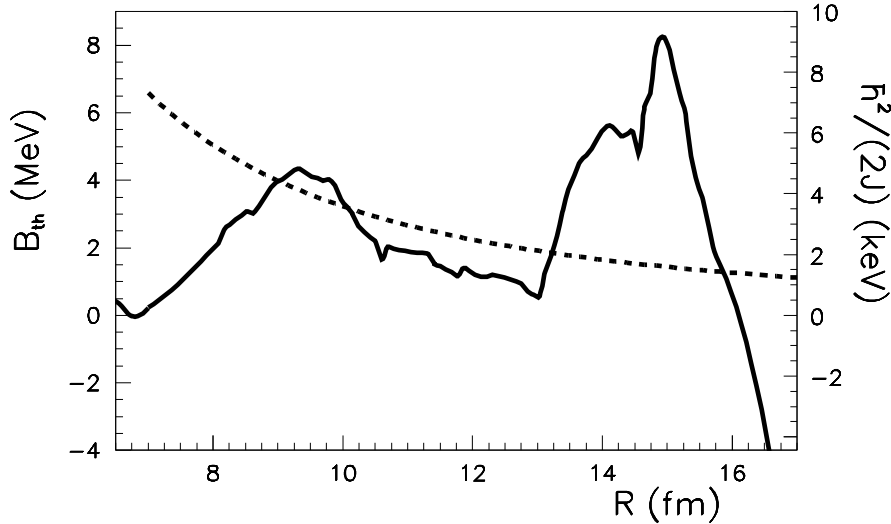


Fig. 2 – Theoretical barrier along the minimal action trajectory as function of the elongation. With the dashed line the constant of inertia is plotted and the corresponding values are displayed on the right scale. Values of the moment of inertia constant close to typical ones are obtained for saddle configurations and wells.

orbit interactions and the  $l^2$  angular momentum interaction. In order to perform the actual calculations the STCSM was drastically improved. In the older version, the spin-orbit and  $l^2$  operators were constructed for a system given by two intersected spheres. In the present version, the spin interactions include a realistic dependence on the neck formed between the nascent fragments.

The barrier obtained after the minimization procedure is plotted in fig. 2 together with the moment of inertia constant  $\hbar^2/(2J)$  where  $J = (A_0/4)R^2$ ,  $A_0$  being the mass of the parent and  $R$  is the distance between the centers of the nascent fragments. The outer barrier is about three MeV lower in energy in the actual version of the STCSM than in the previous one [4, 7]. The barrier exhibits a narrow well in the vicinity of the top of the second barrier. Our efforts are focussed to explain the fine structure without appealing to the occurrence of this phenomenon.

The neutron single-particle level scheme is plotted in fig. 3(a). For elongations comprised between  $R=0$  (spherical shape) and the  $R \approx 7$  fm (fundamental state) the shapes are considered symmetrical by reflection, therefore the parity and the intrinsic spin projection  $\Omega$  are good quantum numbers. From  $R \approx 7$  fm up to the scission, the system loses the reflection symmetry to reach the final partition with  $^{131}\text{Sn}$  heavy fragment and the parity is no longer a good quantum number. Therefore, single-particle interactions can be produced easily between levels characterized by the same value of  $\Omega$ . The spin interaction constants were choosed to reproduce as well as possible the experimental sequence of the first excited levels in the  $^{231}\text{Th}$ . Excepting the  $5/2^-$  bandhead, the first single-particle excited states are retrieved for  $R \approx 7$  fm:  $5/2^+$  (fundamental level), followed by the  $3/2^+$  and  $1/2^+$  excited states. The fundamental state is considered in the present work to have reflection-symmetry. If reflection-asymmetry or mass-asymmetry is considered, the system acquires a doublet structure containing both parities of  $\Omega$ , and the  $5/2^-$  bandhead will naturally appear in the sequence of levels. For the  $^{231}\text{Th}$  compound nucleus, the lowest lying fission channels are essentially low- $\Omega$  single-

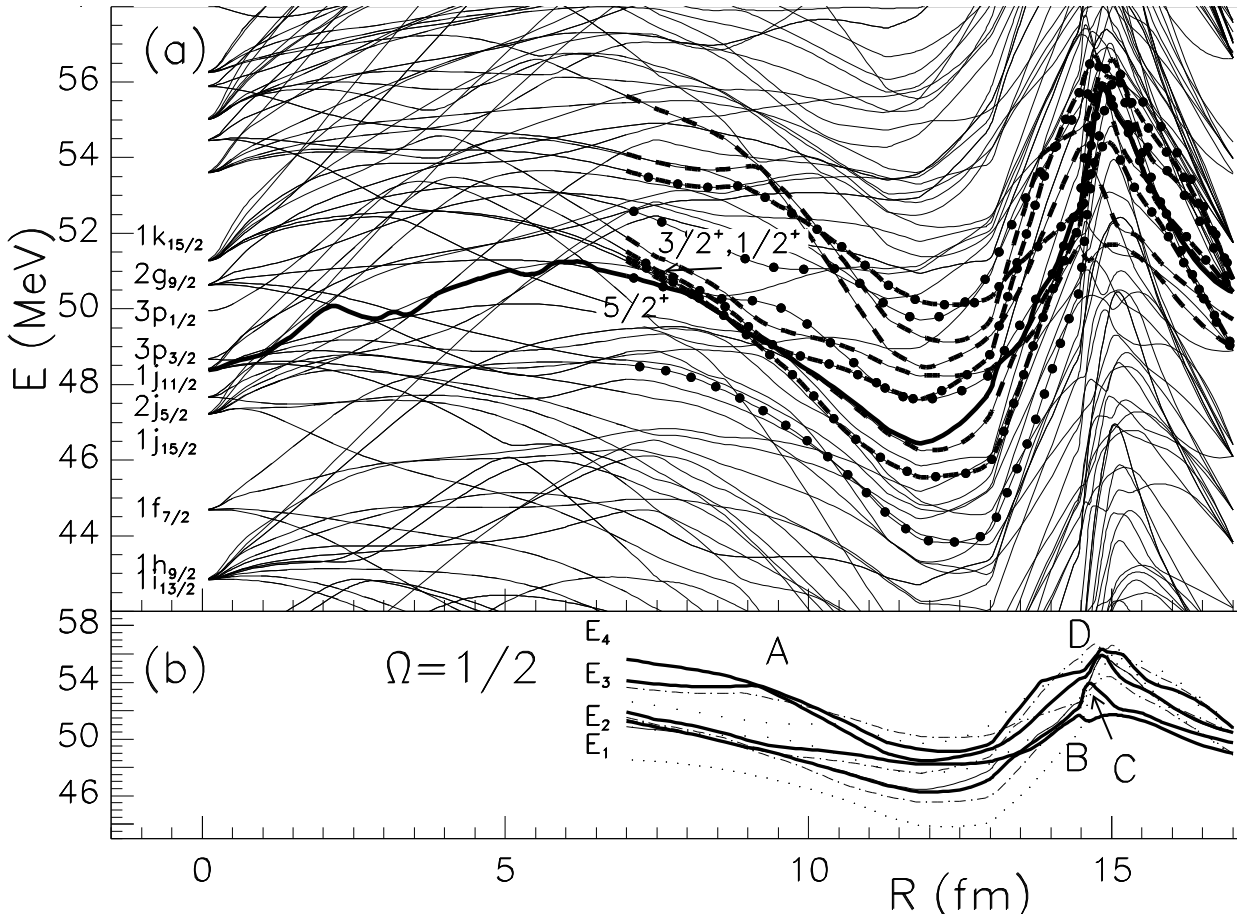


Fig. 3 – (a) Neutron level scheme as function of the elongation. For zero elongation ( $R=0$ ), the shape parameterization describes a spherical nucleus. For low values of the deformations, the system behaves as a Nilsson level scheme. Asymptotically ( $R \rightarrow \infty$ ), the two level schemes of the formed fragments are superimposed. The last occupied level is plotted with a thick full line. Levels of interest are also plotted with different thick line types: dashed line for four  $\Omega=1/2$  levels, dashed-dotted line for three  $\Omega=3/2$  levels, dotted lines for two levels of spin projection  $5/2$  and one of  $7/2$ . The Nilsson parameters  $\kappa$  and  $\mu$  are 0.0637 and 0.74, respectively. (b) The four adiabatic  $\Omega=1/2$  interesting levels are displayed with full thick lines and numbered. The selected avoided crossing regions between  $\Omega=1/2$  levels are marked with letters. The other selected levels and the last occupied one are displayed with narrow lines of same types as in plot (a).

particle states. Higher spins are not allowed by the compound nucleus formation cross section at low energy. Several single-particle levels that lie close to the adiabatic last occupied level are selected as displayed in fig. 3(b). The single-particle levels with the same good quantum numbers associated with some symmetries of the system cannot in general intersect but exhibit avoided level crossings [8,9]. Our system being characterized by an axial symmetry, the good quantum numbers are the intrinsic spin projections  $\Omega$ . The radial coupling causes transitions of the unpaired nucleon from one level to another of same  $\Omega$ . The probability to jump from one level to another can be evaluated by quantifying the Landau-Zener effect with a system

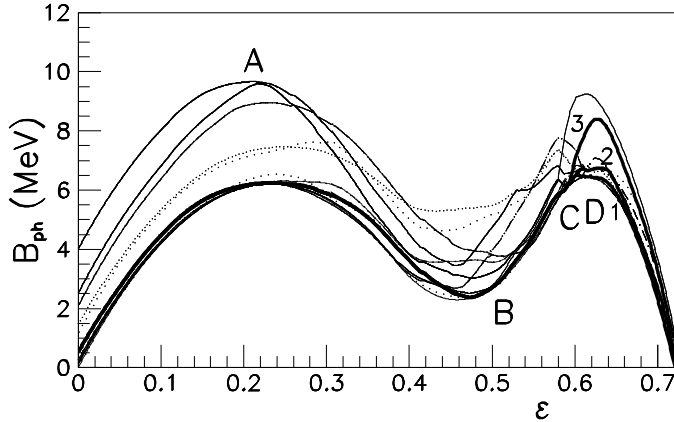


Fig. 4 – Phenomenological barriers with single-particle excitations as function of the dimensionless parameter  $\epsilon$ . The four avoided crossing regions selected for  $\Omega=1/2$  are marked with letters. The three excited  $\Omega=1/2$  selected barriers emerging from the adiabatic level  $E_2$  are plotted with full lines. These barriers are numbered and correspond to excitations as explained in the text.

of microscopic equations of motion as realized in refs. [10, 11]. Solving the coupled channel equations system, the amplitudes of the single-particle wave functions in the nuclear level distribution is determined. In this way, the probability of occupation of an excited level is obtained.

For the four  $\Omega=1/2$  levels, four avoided crossing regions are selected, marked with letters A, B, C and D on the fig. 3(b). If the unpaired nucleon is initially located on the level  $E_1$ , it can follow during the disintegration any of the following paths  $E_2BE_1$ ,  $E_2BCE_2$ ,  $E_2BCDE_3$  or  $E_2BCDE_4$  opened by the avoided crossing regions B, C and D. If the unpaired neutron is initially located on another excited level, different energy paths are open. 18 different excitation channels can be obtained within the selected configuration of only four levels and four avoided crossing regions. In the case of the three  $\Omega=3/2$  selected levels, in a similar manner, 13 different additional excitations are obtained.

The theoretical excitations computed in the frame of the superfluid model are added to a phenomenological barrier. A phenomenological barrier is conventionally simulated within three smoothed joined parabolas [12]. The first barrier is labeled by A, the second one by B and the second well by II. The mixing is realized in the most simplest way by realizing a linear interpolation based on a correspondence between some points  $(R, \epsilon)$  along the  $x$ -axis.  $R$  is the elongation for the theoretical model and  $\epsilon$  the dimensionless parameter used in simulating the phenomenological barrier. The correspondence was choosed for the two minima, the two heights and the exit point. The hybrid model emerges. New barriers are constructed as displayed in fig. 4. An imaginary component of the potential is considered in the second well to take into account other de-excitation channels apart the fission one. The magnitude of this imaginary component increases with the excitation energy of the compound nucleus and it is computed with the recipe of ref. [4]. Finally, the barriers associated to the excitations and their weights are used to determine the cross section by invoking the detailed balance principle.

*Results and discussion.* – After a search of a set of parameters for the phenomenological barrier consistent with experimental data, the neutron-induced cross section is computed.

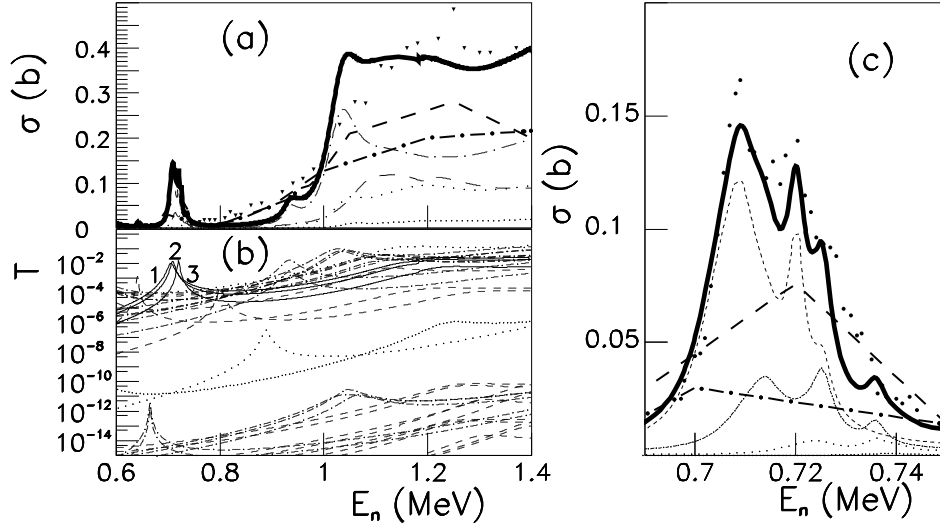


Fig. 5 – (a) Cross section in the threshold region with respect to the neutron energy determined in the frame of HM compared with ENDF/B-VI.8 and JENDF-3.3 [13] evaluations (thick dot-dashed and dashed lines, respectively). Experimental data extracted from ref. [1] are also presented as down-point triangles. The partial contributions in the cross section of different spins of the compound nucleus are displayed with dashed lines for  $I=1/2$  ( $I$  spin of the compound nucleus), dot-dashed lines for  $3/2$  and dotted lines for  $5/2$  and  $7/2$ . (b) Weighted transmissions of the excited barriers that contribute to the total cross section. Same line types are used as in the plot (a) excepting the three transmissions corresponding to barriers 1, 2 and 3 where a full line is used. (c) Detailed representation of the cross section in the region 0.7 MeV. The spin dependent partial cross sections are also given. The ENDF and JENDF evaluations are plotted with dot-dashed and dashed lines, respectively. Experimental data from ref. [2] are also given as full points.

Results are plotted in fig. 5 for the following heights and stiffnesses of the phenomenological barrier:  $V_A=6.24$  MeV,  $V_{II}=2.37$  MeV,  $V_B=6.29$  MeV,  $\hbar\omega_A=0.65$  MeV,  $\hbar\omega_{II}=1$  MeV and  $\hbar\omega_B=1.37$  MeV. In the region  $[0.7, 0.75]$  MeV a fine structure is found by the simulation that agrees very well with experimental data as evidenced in fig. 5(c). Unfortunately, the increasing flank of the cross section around 1 MeV is not well reproduced. Other parameters of the phenomenological barrier succeed to reproduce better this region of the cross section but in the same time lead to a degradation of the quality, for reproducing the cross section behavior around 0.7 MeV. The main question concerns the origin of these fine structure resonances at 0.7 MeV. This structure is produced by very close  $\beta$ -resonances of three excited single-particle barriers of spin  $1/2$  superimposed on resonances due to rotations of the core. The barriers with excitations created by the opened paths  $E_2BCE_2$ ,  $E_2BCDE_3$  and  $E_2BCDE_4$  corresponding to plot 3(b) are marked with the numbers 3, 1 and 2, respectively, on fig. 4. In the vicinity of the top of the second barrier, (the elongation being  $R \approx 15$  fm) a very large density of levels is revealed. This behavior creates premises for an increased number of avoided crossing levels regions and, therefore, for a similar number of small single-particle excitations. The unpaired neutron on the adiabatic level  $E_2$  has a finite probability to jump on the level  $E_3$  at point C and, successively, on the level  $E_4$  at point D (see fig. 3). Three excited barriers are different only in a small interval around the top of the outer barrier up to the exit point, and therefore give three different  $\beta$ -resonance

very close in energy. These resonances are plotted and marked in fig. 5(b) with their respective numbers 1, 2 and 3. These three resonances are in an energy interval smaller than 0.05 MeV and produce three main fine peaks in the fission cross section. Rotational resonances are constructed on these  $\Omega=1/2$  members as described in ref. [4] leading to additional structures. The structure due to rotations can be identified by analyzing the fig. 5(c) where the role played by partial cross sections of spin 3/2, 5/2 and 7/2 can be acknowledged. In the frame of HM, the members of a rotational band are produced by  $\beta$ -resonances in a double barrier modified with a quantity  $E_r(R, L) = L(L+1)\hbar^2/[2J(R)]$ , where  $J(R)$  is the moment of inertia that depends on the elongation (see fig. 2) and  $L$  the orbital momentum of the core.

This investigation shows that the fine structure of the fission cross section can be explained by the existence of several barriers associated to different single-particle excitations. In the case of  $^{230}\text{Th}$  neutron-induced fission, an unpaired neutron follows a well defined single-particle adiabatic level during the deformation process and it is excited on other adiabatic levels in the vicinity of the top of the second barrier, where the level density is very high. That causes the apparition of several peaks very close in energy in the cross section. It can be assessed that dynamical single-particle effects can be responsible for the fine structure phenomenon in the induced fission cross section.

In the ref. [3], it was evidenced that a good fit of the 0.7 MeV resonance behavior can be realized only by taking into account two spin 1/2 bandhead resonances created by slightly different barrier parameters in the three humped picture. In the actual model, these bandheads appears naturally and the variation of the barrier parameters are justified by the existence of excitations close to the top of the barrier. It can be also underlined that the actual evaluations of data files, as evidenced by the large discrepancies revealed in fig. 5, fail to reproduce the fine structure.

As a general conclusion, it is possible that the complex resonant structure of the fission cross section is due to a rearrangement of orbitals and to the dynamics of the process, beginning from the ground-state of the compound nucleus and reaching the scission. A large number of different excited barriers are formed leading to a large number of vibrational resonances in the second well. So, these resonances carry information about the structure of the nucleus and the dynamics.

## REFERENCES

- [1] JAMES G.D., LYNN J.E. and EARWAKER L.G., *Nucl. Phys.*, **A189** (1972) 225.
- [2] BLONS J., MAZUR C., PAYA D., RIBRAG M. and WEIGMANN H., *Phys. Rev. Lett.*, **41** (1978) 1282.
- [3] BOLDEMAN J.W., GOGNY D., MUSGROVE A.R. DE L. and WALSH R.L., *Phys. Rev.*, **C22** (1980) 627.
- [4] MIREA M., TASSAN-GOT L., STEPHAN C., BACRI C.O., STOICA P. and BOBULESCU R.C., *J. Phys. G*, **31** (2005) 1165.
- [5] POENARU D.N., IVASCU M. and MAZILU D., *Comput. Phys. Commun.*, **19** (1980) 205.
- [6] MIREA M., *Phys. Rev.*, **C54** (1996) 302.
- [7] MIREA M., TASSAN-GOT L., STEPHAN C. and BACRI C.O., *Nucl. Phys.*, **A735** (2004) 21.
- [8] PARK J.Y., GREINER W. and SCHEID W., *Phys. Rev.*, **C21** (1980) 958.
- [9] CHA M.H., PARK J.Y. and SCHEID W., *Phys. Rev.*, **C36** (1987) 647.
- [10] MIREA M., *Phys. Rev.*, **C57** (1998) 2484.
- [11] MIREA M. and CLAPIER F., *Europhys. Lett.*, **40** (1997) 509.
- [12] CRAMER J.D. and NIX J.R., *Phys. Rev.*, **C2** (1970) 1048.
- [13] <http://www.nndc.bnl.gov/index.jsp>